Embedded deep-learning based sample-to-answer device for on-site malaria diagnosis

Chae Yun Bae[1$], Young Min Shin[1$], Mijin Kim[1$], Younghoon Song[1$], Hong Jong Lee[1], Kyung Hwan Kim[1], Hong Woo Lee[1‡], Yong Jun Kim[1], Creto Kanyemba[2], Douglas K Lungu[2], Byeong-il Kang[1§], Seunghee Han[1||], Hans-Peter Beck[3,4], Shin-Hyeong Cho[1,5], Bo Mee Woo[1], Chan Yang Lim[1]*, Kyung-Hak Choi[1]*

1. Noul Co., Ltd. Yongin-si, Gyeonggi-do, Republic of Korea
2. Wezi Medical Centre; Box 716, Mzuzu, Malawi
3. Department of Medical Parasitology and Infection Biology, Swiss Tropical and Public Health Institute, Allschwil, Switzerland
4. University of Basel, Basel, Switzerland
5. Department of malaria and parasitic diseases, Korea Centers for Disease Control and Preventions (KCDC), Cheongju-si, Chungcheongbuk-do, Republic of Korea

[$]Co-first author
*Co-corresponding author

‡Hong Woo Lee is now affiliated with Woven by Toyota, Tokyo, Japan. The research for this paper was conducted while he was affiliated with Noul Co., Ltd.

§Byeong-il Kang is now affiliated with Beckman Laser Institute Korea, Dankook University, Cheonan, Republic of Kora. The research for this paper was conducted while he was affiliated with Noul Co., Ltd.
||Seunghee Han is now affiliated with Medithings Inc. Seoul, Republic of Korea. The research for this paper was conducted while he was affiliated with Noul Co., Ltd.

Corresponding author

Kyoung-Hak Choi, PhD
Noul Co., Ltd.
Yongin-si, Gyeonggi-do, Republic of Korea
Phone: +82-10-3322-4911
E-mail: kaleb@noul.kr

Abstract

In response to the ongoing global health problem caused by malaria, especially in resource-limited settings, digital microscopy must be improved to overcome the limitations associated with manual microscopy. In order to present a malaria diagnosis method that is not only accurate at the cell level but also clinically performs well, improvements in deep-learning algorithms and consistent staining results are necessary. The device employs a solid hydrogel staining method for consistent blood film preparation, eliminating the need for complex equipment and liquid reagent maintenance. By leveraging deformable staining patches, the miLab™ ensures consistent, high-quality reproducible blood films can be made across various hematocrits. Embedded deep-learning enables the miLab™ to detect and classify malaria parasites from the autofocused images of stained blood cells by internal optical system, achieving a high correlation with manual microscopy images. This innovation not only minimizes human error but also facilitates remote assistance and review by experts through digital image transmission, revolutionizing the landscape of on-site malaria diagnosis. The miLab™ algorithm for malaria detection shows a total accuracy of 98.83% for infected RBC classification. Clinical validation in Malawi demonstrates an overall percent agreement of 92.21%, highlighting the miLab™'s potential as a reliable and efficient tool for decentralized malaria diagnosis.

Keywords

Malaria diagnosis, Microscopy examination, Digital microscopy, Automated staining process, Deep-learning algorithms

Introduction

Malaria continues to pose a formidable threat to global public health, with over 247 million reported cases and 593,000 related deaths in 2021(World malaria report 2021, 2021). The overwhelming majority of malaria incidents, exceeding 99%, are concentrated in low- and middle-income nations, with 95% occurring in Sub-Saharan Africa. Despite the advantages offered by cost-effective Rapid Diagnostic Tests (RDTs) and the precision of Polymerase Chain Reaction (PCR), malaria diagnosis has traditionally relied on manual microscopy, coupled with visual inspection by highly trained experts. Manual microscopic examination is recommended because of its robustness in eliminating false-positive or false-negative results(Beck, 2022; Fitri et al., 2022). However, the quality of microscopy-based diagnosis is largely affected by the smearing and staining quality, and the expertise of microscopist who reads the smeared blood slides. These malaria-endemic countries lack adequate healthcare facilities, reagents, trained professionals, vector control, and surveillance systems, which hinder malaria eradication(Oduola et al., 2018; Sori et al., 2018; Gaston and Ramroop, 2020).

To overcome these obstacles of manual microscopy examination in malaria diagnosis, digital microscopy and the computational image analysis algorithms have been proposed(Mody et al., 2006). The diagnosis based on the digital image can reduce human labor, give aid to local healthcare workers, and enable experienced experts in remote locations to review the microscope. Recent advances in image analysis techniques based on the deep-learning(Krizhevsky et al., 2012) made this approach more affordable by virtue of the higher accuracy compared to the traditional machine learning algorithm(Liang et al., 2016; Gopakumar et al., 2018; Rajaraman et al., 2019; Zhao et al., 2020; Li et al., 2021; Meng et al., 2022; Madhu et al., 2023). However, these studies only conducted cell-level evaluation in the datasets without clinical tests(Liang et al., 2016; Gopakumar et al., 2018; Rajaraman et al., 2019; Molina et al., 2020; Zhao et al., 2020; Li et al., 2021; Meng et al., 2022; Madhu et al., 2023), leaving doubts about their performance in real environments. A few papers reported patient-level malaria diagnosis using image analysis in

clinical settings, but their accuracy required further improvements(Yoon et al., 2019; Das et al., 2022). Although computer algorithms have great advantage over human readers in terms of consistency, their performance is significantly affected by slide quality(Das et al., 2022). This suggests that computer algorithms need to be scaled up much further with more datasets to overcome their dependency on the blood film preparation quality and adapt to the variability of slides.

The performance of traditional machine learning algorithms tends to get saturated easily as the training data increases. On the contrary, deep-learning algorithms can learn from larger datasets to train much bigger models to attain better accuracy. This trend has continued after the emergence of deep-learning; the best model for image classification had 62 million trainable parameters in 2012(Krizhevsky et al., 2012) and the number of parameters increased up to 2,44 trillion in 2022(Wortsman et al., 2023). Accordingly, the required computational resources also had to grow to accommodate the larger models. The cloud computing or server-level computing is generally used to run the current large state-of-the-art models. Nevertheless, employing large deep models that require powerful computer or stable internet connection is not a feasible solution in malaria endemic countries. Instead, embedding efficient deep-learning model into the portable device is beneficial to use the device in real clinical environments, also consistent blood film preparation is essential to achieve high accuracy by reducing the image domain space.

Here, we introduce the miLab™, an embedded deep-learning based sample-to-answer device for on-site malaria diagnostics capable of handling automated blood film preparation and autofocused imaging with digital microscopy (Figure 1A). We provided a quick, inexpensive, and environment-friendly method to stain smears with dyes using deformable staining patches (Choi et al., 2021; Bae et al., 2023) and validated consistent, high-quality, thin smears for blood samples over a broad range of hematocrits. The embedded deep-learning algorithm analyzed malaria suspected morphology from the blood cells stained in this device and the autofocused digital images were taken by the optical system of the same device. Digital microscopy of the device for

on-site malaria diagnosis can also scan more than 200,000 Red blood cells (RBCs) around 7 to 10 minutes without any confusing human error. Therefore, this innovative device allows on-site users to analyze digital image data on the spot, obtaining immediate diagnostic results without the need for high-performance computing. At the same time, digital images can be sent to experts to assist with diagnosis even from remote locations (Figure 1B). On-site users can immediately check the suspected morphology of the malaria by deep-learning through the screen mounted on the device (Figure 1C), and other experts can access the same digital images on a web-based software to review those suspected morphology and the diagnostic results (Figure 1D). The embedded deep-learning based on-site malaria diagnostic platform not only provides the same experience as in-person microscopy examination in the laboratory, but also creates the possibility of remote diagnosis.

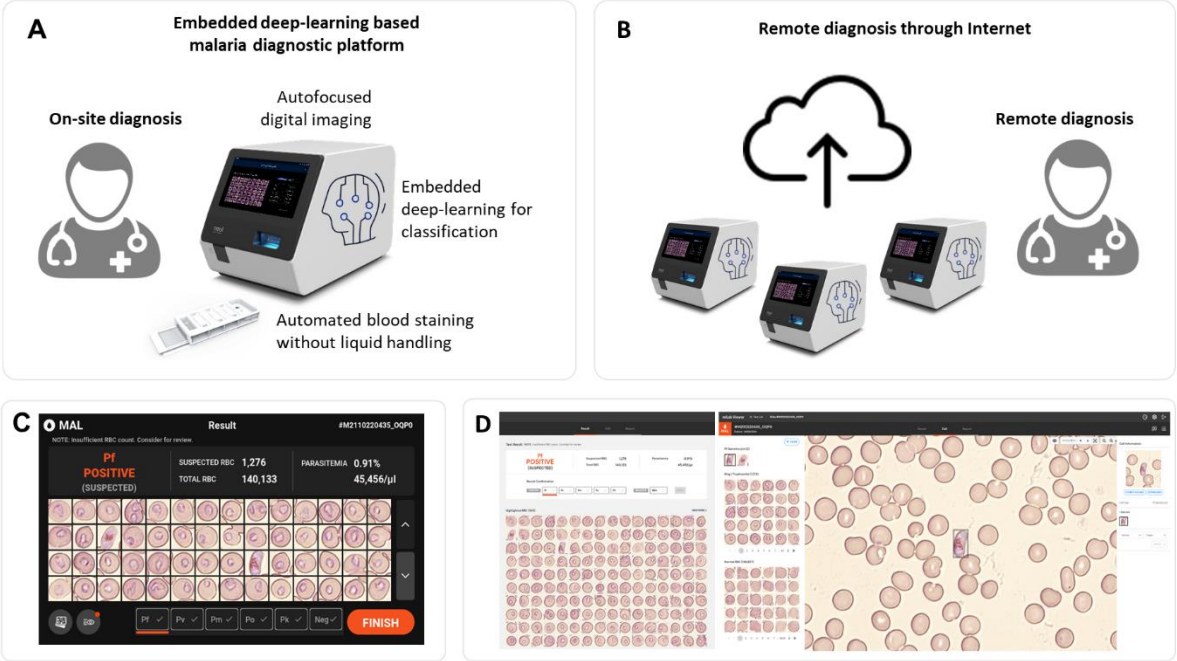

Figure 1 Schematic of the embedded deep-learning based on-site malaria diagnosis. (A) The miLab^{TM} not only automates the entire process (automated blood staining without liquid handling and autofocused digital images) of malaria diagnosis through microscopic analysis but also incorporates deep-learning algorithm directly into the device for on-site review. (B) A web-based software allows to access the digital images for the experts to remotely review the result through the internet. (C) Picture of the result page in the miLab^{TM} for the *P.falciparum* positive patient specimens. Users can review and confirm the results in the miLab^{TM} for sample-to-answer, on-site malaria diagnosis. (D) Picture of the screen shot of the result page from the same patient speciemens on the web-based software, accessing remotely digital images and raw data from the miLab^{TM}. Other experts can remotely review and confirm the same results from the miLab^{TM}.

Materials and Methods

Ethical approval for blood sample

Whole blood samples used for blood film in miLab™ validation were collected for research purposes only and approved by the Institutional Review Board (P01-202003-31-007, and GCL-2020-1011-01) of the Korea National Institute for Bioethics Policy (Seoul, Korea) and GCLabs (Yongin, Korea). Clinical samples (n=555) which were analyzed in two miLab™ devices were collected from April 2022 to November 2022 were used in the clinical validation study which approved by the Institutional Review Board (IRB00003905) of the National Health Sciences Research Committee (Ministry of Health, Malawi). After explaining the purpose of the study, the procedure, possible benefits, risks, and rights of the participants, all subjects were requested to voluntarily sign the informed consent forms.

Validation of the blood film in the miLab™

The hematocrit of the blood sample was measured using a hematocrit-measuring instrument (Boditech Med Inc., FPRR005). The performance of preparation of the blood film in the miLab™ (212 mm (w) x 390 mm (l) x 244 mm (h). w; width, l; length, h; height) was validated based on the number, morphology, and color of stained RBCs prepared. Images of stained RBCs prepared using clinical specimens were captured in miLab™, and field of views (FoVs) filled with stained RBCs were acquired. The embedded deep-learning algorithm segmented the RBCs from the background of the FoVs. The number of RBCs in a FoV was determined, and the red, green and blue (RGB) values were obtained from the pixels of the segmented RBCs. To evaluate the reproducibility of blood films in miLab™, the embedded deep-learning algorithm counted the number of segmented RBCs in each FoV. The mean RBC counts from 50 FoVs of 20 replicate slides for 7 specimens were used to examine the precision of smear generation. To evaluate reproducibility of blood films staining by miLab™, the mean RGB value from the entire region of segmented RBCs was used as the representative RGB value in a FoV. Two hundred FoVs per specimen were used to examine the color of the specimen by calculating the mean, standard

deviation, and coefficient of variance. To examine morphological features of *Plasmodium* in the blood film from the miLab™, four different types of typical stages and species (ring for early trophozoite, late trophozoite from *P. vivax*, gametocyte from *P. falciparum* and *P. vivax*) were collected from the miLab™ and the manual Giemsa staining method using a mixture of eosin and methylene blue. Each morphology was also observed from the miLab™ and under the microscopy (CX33 with 50x objective lens, Olympus).

Validation of embedded deep-learning algorithm in the miLab™

The performance of embedded deep-learning algorithm in the miLab™ was validated using the correlation between malaria-positive RBC counts obtained by conventional microscopy and by miLab™. In total, 3,000 FoVs from 15 malaria-positive clinical specimens (200 FoVs each) were annotated by an experienced microscopist. Among these, 1,803 were confirmed to be malaria positive. These were analyzed using the classifier embedded in miLab™. In each of the FoVs, the number of RBCs determined as malaria-positive by the classifier was compared to that annotated by the microscopist using Pearson's correlation analysis.

Clinical validation

Samples (n=555) from Wezi Medical Centre and Mapale Health Center (Mzuzu, Malawi) were collected for determining the malaria diagnostic performance of miLab™. Two miLab™ devices were used to analyze these samples from April 2022 to November 2022. The results obtained by miLab™ were compared with reference tests, such as microscopic examination by an experienced local microscopist in Malawi and alongside with RDT (CareStart™ Malaria Pf (HRP2) Ag RDT, AccessBio, NJ). Blood samples (~250 µL) were collected into blood capillary tubes by finger prick using a sterile lancet and stored in an anticoagulant tube with ethylenediaminetetraacetic acid (EDTA). 5 µL of the collected blood were used to prepare both a thick and a thin blood film for microscopic examination. This blood film was stained with a mixture of eosin and methylene blue using the manual Giemsa staining method. Local microscopists

examined the Giemsa-stained slides with an Olympus CX33 microscope according to the standard microscopy methods of the WHO(World Health Organization & UNICEF/UNDP/World Bank/WHO Special Programme for Research and Training in Tropical Diseases, 2015).

Statistical analysis

All statistical analyses were performed using GraphPad Prism (Ver.7, GraphPad Inc., San Diego, CA, USA). To evaluate correlation, linear least squares analysis was performed at the 95% confidence interval of each variable, and the Pearson correlation coefficient was calculated. Differences between groups were examined using Student's unpaired t-test. All analyses were performed using a two-sided test, and the results were considered statistically significant at $p < 0.05$.

Results

Repeatable preparation of the blood film in the miLab™

This is a relatively simple staining method which requires just 5 μL of blood sample to be used in the miLab™ device which is a bench-top device for staining tens of thousands of RBCs and *Plasmodium* species. We employed a solid staining method using hydrogel, eliminating the need for controlling complex equipment or maintenance of liquid reagents(Choi et al., 2021). This approach involves bringing hydrogel into contact with appropriately smeared and fixed cell surfaces, allowing the dye to efficiently stain the cells. The amount of dye from the hydrogel is applied on to the smear in a very short time, under one minute, depending on the type of dye used(Bae et al., 2023). In addition, hydrogel without dye can absorb any remaining dye on the cell surface and attain suitable staining quality depending on the pH of the buffer in the hydrogel like the role of conventional buffer solution in blood cell staining(Oktiyani et al., 2022). Each cartridge consists of a spreader film for preparing blood film and three different types of staining patches, facilitating consistent RBCs smearing and staining (Figure 2A). The cells can be smeared and stained by simply moving the blood-loaded cartridge without any controlling of

aqueous solution. In this way, automated processes for blood film can be designed to stain the morphology of *Plasmodium* effectively and appropriately on-site.

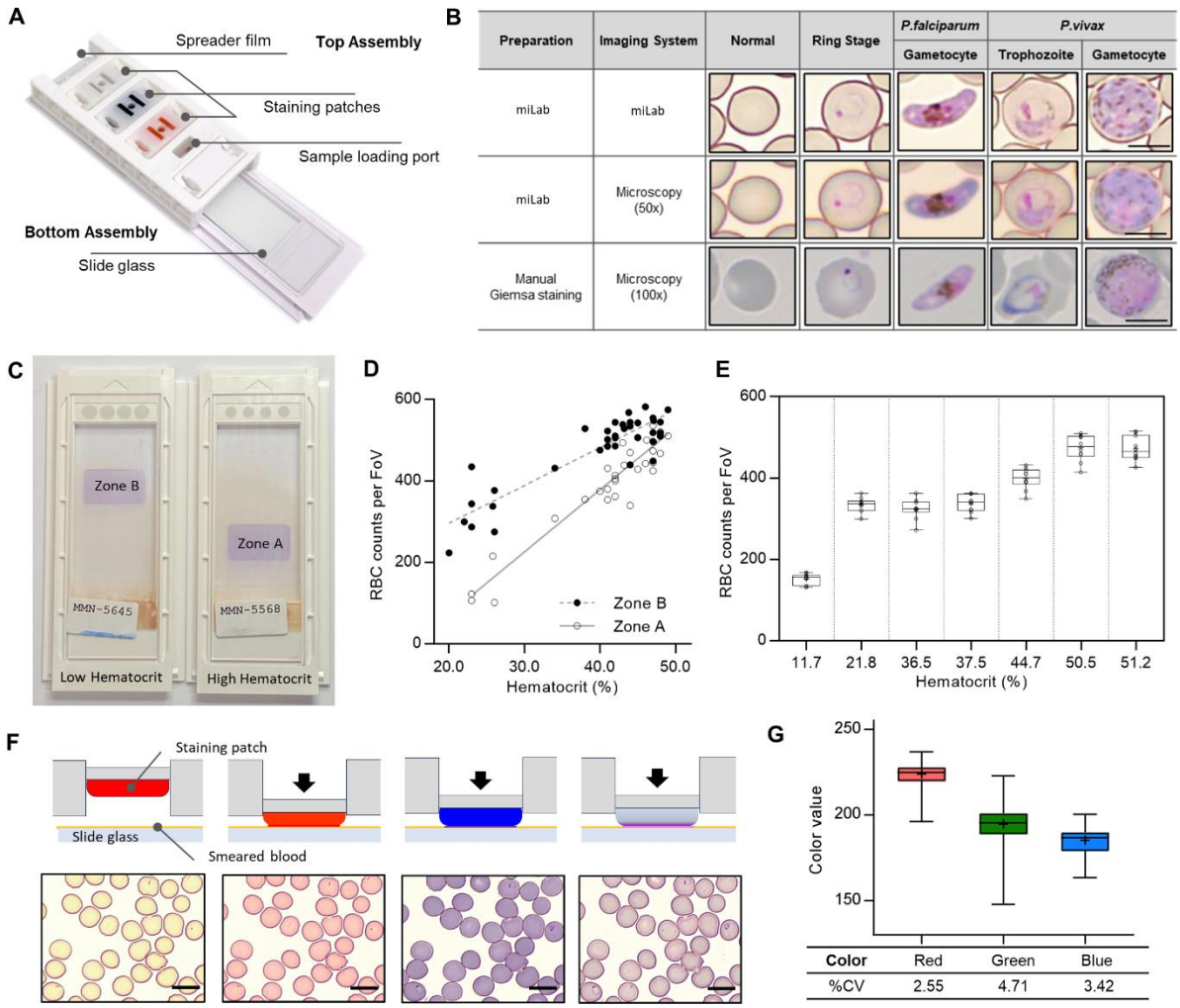

Figure 2 Validation of the blood film in the miLab^{TM}. (A) Picture of the miLab^{TM} cartridge. It consists of top assembly and bottom assembly. 40 mm (w) x 92 mm (l) x 15 mm (h). w; width, l; length, h; height. (B) Comparison of microscopic cell image with miLab^{TM} blood film acquired from the miLab^{TM}, 50x olympus microscopy with miLab^{TM} blood film, and 100x microscopy with conventioanl Giemsa slides. The scale bars = 5 µm. (C) Picture of the prepared blood films from the miLab^{TM} using a patient specimens with low hematocrit and high hematocrit from Malawi. Low hematocrit samples needed to be read in Zone B instead of Zone A, where high hematocrit samples were typically read. The miLab^{TM} device automatically detects an appropriate area to observe RBCs in a monolayer. (D) Correlation of average RBC counts per FoV depending on the hematocrit of the clinical specimens (n = 37) was shown with open dots (Zone A) and close dots (Zone B). € Reproducibility of blood smear was represented with box plot using RBC counts per FoV in seven clinical specimens (n = 20). Average RBC counts per FoV were demonstrated with low, middle and high hematocrits. The RBC counts of the samples with the low (< 30%) and the middle/high hematocrits (> 30%) were selected from Zone B and Zone A, respectively. (F) Schematic of blood staining using three distinct staining patches in the cartridge and pictures of stained blood cells with *Plasmodium* infected RBCs dfrom each steps of staining procedure. The scale bars = 10 µm. (G) Reproducibility of blood staining was represented with box plot using the red, green, and blue color value which was obtained from the stained RBCs in FoVs of clinical specimens. Each of the RGB color values was conserved across FoVs (n = 4,000).

The optical system of the device automatically scans the results of stained blood cells. By considering the size and location of stained parasites within RBCs, the optical system rapidly captures autofocused images through ten different focal planes. This provides a clear morphology of *Plasmodium* at each stage, similar to the conventional microscopy examination using Giemsa staining for 100x microscopy images (Figure 2B). In particular, when comparing images of *Plasmodium* morphologies stained by the cartridge with manually focused images at the same resolution using a 50x microscope, their distinctions in the morphology and species were discernible even in the auto-focused images within the device. These digital images not only allow the embedded deep-learning algorithm to detect malaria on-site but also enable experts to distinguish between types and stages of malaria through the result screen in the device or viewer at remote locations.

To ensure accurate diagnosis, it is crucial to obtain digital images that demonstrate reproducible automated preparation processes and effectively depict the morphology of *Plasmodium*. Therefore, we verified the consistency of RBC counts and color difference when performing the automated preparation processes in the miLab™. To address the unique characteristics of malaria patients with lower RBC counts, we implemented a two-speed smearing process on the spreader with a consistent angle, screening an adequate number of RBCs in low-hematocrit samples ranging from 20% to 35%. This provided two different zones for detecting appropriate RBCs depending on the hematocrit of the samples (Figure 2C). When we investigated the correlation between average RBC counts per FoV depending on the hematocrit from the 37 clinical specimens, each zone A and zone B showed linear correlation of RBC counts compared to hematocrit (Figure 2D, Supplementary Figure 1). The RBC counts of the samples with the low (< 30%) and the middle/high hematocrits (> 30%) was selected from Zone B and Zone A, respectively. To increase the efficiency of RBC screening, RBCs from low hematocrit samples can be screened in zone B (average 200~400 RBC counts per a FoV) instead of zone A (average 100~300 RBC counts per a FoV). The screening of RBCs performed on a variety of hematocrit

samples, including 20~50%, also resulted in a CV% of less than 10%, even in 20 replicates of 7 clinical specimens (Figure 2E).

Because three-color values are the most common color space for segmenting parasites and RBCs from thin blood film (Fong Amaris et al., 2022), each RGB value was extracted from segmented RBCs and quantitatively analyzed for appropriate blood smear and staining. Depending on the types of staining patches which included different types of Romanowsky stains such as Eosin, Methylene blue and Azure B, the color of RBCs and even morphology of parasites were observed differently (Figure 2F). Compared to the pre-stained images, the transparent patch is responsible for absorbing the dye, while the dye-containing patches mainly serve to release the dyes into the cells. Figure 2G summarizes the analysis of the color values of the stained images. The CV% of the three-color values over a total of 4,000 FoVs was found to be less than 5% and was maintained across 200 FoVs for each blood film (Supplementary Figure 2). Hydrogel stamping-based staining thus precisely controls the color of the stained blood cells and performs blood film preparation efficiently and reproducibly.

High accuracy of malaria detection at cellular level on embedded deep-learning algorithm in the miLab™

A machine learning algorithm was applied to analyze the captured images and detect malarial parasites in the blood. To identify the presence of rarely infected RBCs, we devised a two-step image analysis algorithm that includes RBC detection and subsequent classification. The sub-images were extracted from the entire image to obtain one RBC for each event (1st step: detection). Then, each of the cropped sub-images was tested for the presence of the malarial parasite (2nd step: classification). The two-step algorithm divides images into meaningful units and analyzes each unit in detail, instead of trying to find scarce malaria parasites directly in the vast number of images. To incorporate the machine learning model into the limited resources of the embedded hardware, all the neural network architectures were designed to reduce computational complexity. Because our target images were full of RBCs, we adopted a semantic

segmentation algorithm instead of a general object detection algorithm to achieve compactness and efficiency(Olaf Ronneberger et al., 2015; Tran et al., 2019; K.T. et al., 2022).

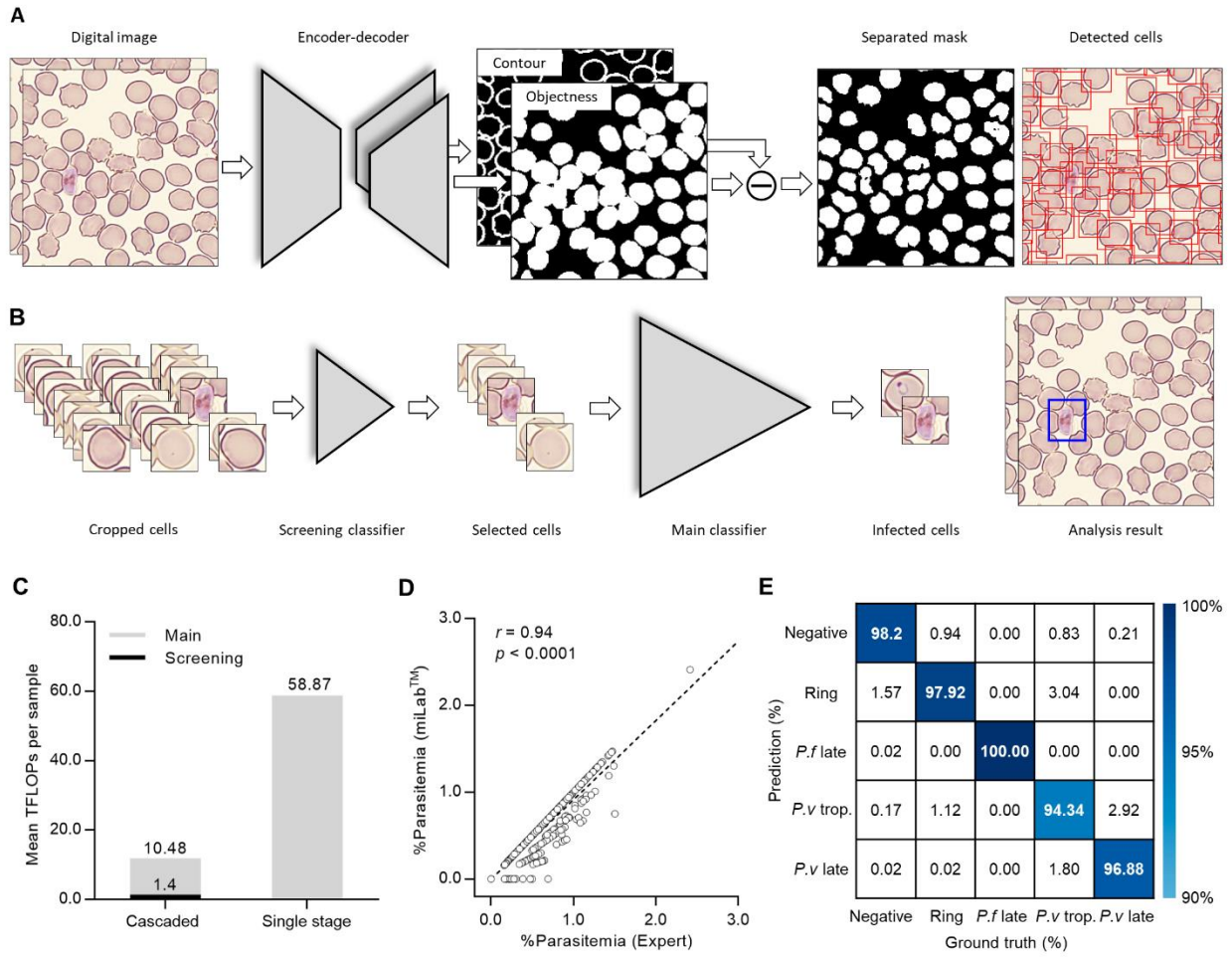

Figure 3 Performance of embedded deep-learning algorithm in the miLab^{TM} at the cellular level. (A) Our segmentation network has one common encoder and two decoder branches. The network is trained to assign objectness value 1 when the corresponding pixel is on the foreground object, while the contour is trained to fire on the boundary of cells. The aggregated cells are separated by subtracting the contour image from the objectness image. (B) The cascaded neural network classifies the cropped RBCs. (C) Although the cascaded classifiers have an additional screening classifier prior to the main classifier, the single stage classifier consumes ~5 times more total computational cost to classify the RBCs. (D) Correlation of the proportion of malaria parasite-infected RBCs between conventional microscopy and the miLab^{TM}. The Pearson's correlation method was used to evaluate the correlation. (E) AI model validation for stage classification was represented using the confusion matrix. (*P.f* late; gametocyte, *P.v* trop.; trophozoite, *P.v* late; schizonts or gametocyte)

After automated image acquisition, the miLab^{TM} uses a semantic segmentation algorithm designed to produce two outputs as segmentation mask images, namely, objectness and contour. After running the semantic segmentation algorithm, the contour image was subtracted from the objectness image to exclude aggregated cells. Cell locations were determined by analyzing the

connected components from the resulting segmentation masks (Figure 3A). The detected blood cells were cropped and passed through the classification module. Because the number of detected cells was large, and uninfected cells were the dominant component, it was not efficient to pass all cells through the entire classification procedure. Therefore, our classification module comprises two cascaded classifiers to reduce the computational burden imposed by the skewed ratio of parasite-positive to -negative cells (Figure 3B). The first classifier consists of only 3 convolutional layers and screens for obviously “clean” uninfected cells. If a cell is classified as clearly uninfected, it is not passed onto the second classifier. This prior “screening” classifier considerably reduces the number of cells delivered to the subsequent classifier. The second “main” classifier performs an in-depth examination of only those cells deemed by the first classifier to be possibly infected. The second classifier is based on the ResNet(He et al., 2016) architecture and is equipped with a convolutional block attention module (CBAM)(Woo et al., 2018). Like our segmentation network, the main classifier has a multi-task learning framework that predicts the presence of malaria and estimates its developmental stage. In our verification study, only 17.8% of the RBCs passed the screening classifier and were delivered to the main classifier, whereas the conventional monolithic classifier had to examine all RBCs (Figure 3C). The current AI of miLab™ can detect malaria parasite-infected RBCs in the operator-assigned number (default: 200,000) of RBCs and classifies developmental stages based on their morphology: *P. falciparum* and *P. vivax* ring stage, *P. falciparum* late-stage (i.e. gametocyte), *P. vivax* trophozoite stage, and *P. vivax* late-stage (i.e. schizont and gametocyte). The performance for detecting infected RBCs was verified using blood films prepared from 15 clinical specimens that were determined to be positive for malaria. We randomly selected 200 FoVs for each blood film and compared the proportion of infected RBCs from the miLab™ to microscopic results obtained visually. There was an excellent correlation between the results from both methods, with a Pearson’s correlation coefficient (r) of 0.94 ($p < 0.0001$; Figure 3D). Finally, the performance for stage classification was confirmed using 11,718 single-cell images acquired from blood films prepared by the miLab™,

where the stages were determined independently by expert microscopists. Figure 3E shows the confusion matrix from the verification study for multi-stage malaria parasite classification. The total accuracy for the classification of infected RBCs was 98.83% (95% CI: 98.62–99.01%) and that for the classification of *Plasmodium* species and stages was 97.82% (95% CI; 97.53–98.06%). The algorithm of the miLab™ shows excellent performance in malaria detection with identification of multiple stages of the parasite's life cycle in this analytical validation study.

We set a threshold value to the output score of the classifier that represents a suspected malaria infection, based on the morphology of each cell. In the miLab™ algorithm, a cell was considered malaria-positive if its score was higher than the threshold, and negative if it was below the threshold.

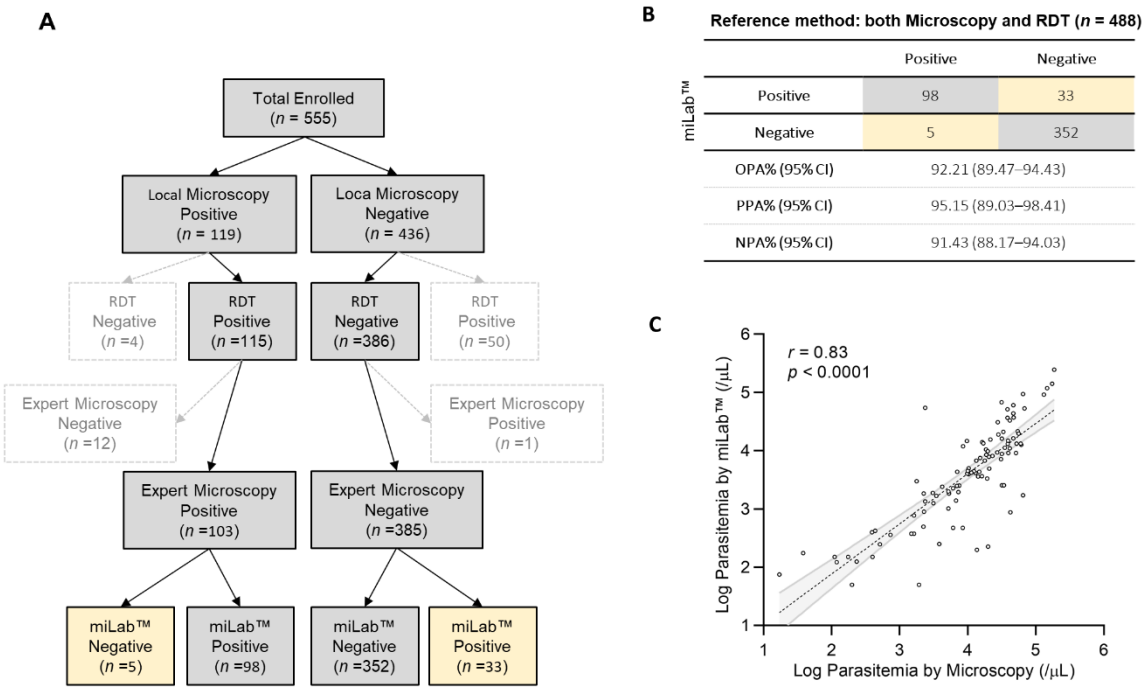

Figure 4 Clinical validation of the miLab™ in Malawi. (A) Design for a clinical study. A total of 555 clinical specimens was enrolled and subjected to microscopy and analysis by the miLab™ for comparison with the reference tests (both local microscopy examination and RDT). Yellow cells indicate samples discordant with the reference test. (B) Agreement of analysis by the miLab™ with the reference tests (microscopy and RDT). Based on the concordance of microscopy and RDT, overall percent agreement (OPA), positive percent agreement (PPA) and negative percent agreement (NPA) were 92.21%, 95.15%, and 91.43% respectively. (C) Correlation of parasitemia level between microscopy and the miLab™ on a logarithmic scale. The Pearson's correlation Coefficient (*r*) is 0.8259 (95% CI: 0.7518 to 0.8794).

Evaluation of Clinical Performance in Malawi

The clinical performance of the miLab™ was evaluated using 555 patients speciemens that were prospectively collected from patients with fever who visited the clinical study site, Mzuzu Health Centre in Malawi, where the predominant species is *P. falciparum*(Gaston and Ramroop, 2020; U.S. President's Malaria Initiative Malawi Malaria Operational Plan FY, 2020). The clinical information of the patients was summarized in Supplementary Table 1 and 2. Figure 4A shows the study design for clinical validation of the miLab™, based on the approved study protocol. We set a threshold value to the output score of the classifier that represents a suspected malaria infection, based on the morphology of each cell. In the embedded deep-learning algorithm, a cell was considered malaria-positive if its score was higher than the threshold, and negative if it was below the threshold. When we analyzed 488 clinical specimens by the miLab™ after excluding 67 samples with discrepancies between reference tests, an overall percent agreement (OPA) of 92.21% (95% confidence interval (CI); 89.48–94.43%), positive percent agreement (PPA) of 95.15% (95% CI; 89.03–98.41%), and negative percent agreement (NPA) of 91.43% (95% CI; 88.17–94.03%) were found (Figure 4B).

The miLab™ results were compared for concordance with manual microscopy and RDT as reference tests. Figure 4C shows the correlation of parasitemia between manual microscopy and the miLab™. The mean parasitemia of positive samples is approximately ~26,000 (parasites per µL) from the miLab™ and ~22,000 (parasites per µL) from the microscopist. Since the miLab™ quantifies parasitemia based on 5,000,000 RBCs per µL of the blood, parasitemia from patients with abnormal RBCs or WBCs outside the range may differ from quantification based on 8,000 WBCs per µL of blood through the conventional microscopy examination. Nevertheless, the parasitemia value determined by miLab™ in the Pearson's correlation coefficient (r) of (0.8259, 95% CI; 0.7518–0.8794) showed excellent agreement with the quantification results obtained by the microscopist.

Discussion

On-site, sample-to-answer malaria diagnosis in the miLab™ enables blood film preparation for embedded deep-learning based malaria detection using digital microscopy images. The miLab™ applies hydrogel staining patches for the blood films generation in a highly reproducible manner. This on-site diagnostic platform with A4 paper-sized footprint also applied ethanol-based fixation to avoid the use of methanol and staining patches to reduce liquid wastes without maintaining reagents for user safety and convenience. There is no need for a sophisticated and well-equipped central laboratory. The miLab™ device functions as a stand-alone unit that can be deployed in resource-limited environments. Validation of the system showed excellent reproducibility in blood film preparation (Figure 2D, 2E, 2G, Supplementary Figure 2). The accuracy of deep-learning based analysis in cellular level was comparable to that of other research groups(Liang et al., 2016; Shen et al., 2017; Gopakumar et al., 2018; Rajaraman et al., 2019; Zhao et al., 2020; Li et al., 2021). This consistent performance and higher accuracy of the miLab™ eliminated the dependency on technicians for manual microscopy-based malaria diagnosis by providing both blood film preparation and automated analysis, compared to other products (Yoon et al., 2019; Das et al., 2022).

The clinical performance evaluation of the miLab™ using 488 clinical specimens resulted in an overall percentage agreement (OPA) of 92.21% before user reviews. Out of 488 analyzed samples, 38 samples (7.79%) were discordant with the reference tests as false negatives or false positives. When users review the results either on the device or on the web-based software, the ‘review needed’ or ‘suspected’ morphology of the parasites would appear on the miLab™ read-out. In this clinical validation study, users would need to review the raw data and confirm the diagnostic results for 131 (including 98 true positive and 33 false positive) among 488 patient specimens. Clinical performance may vary slightly depending on the device's threshold setting. Choosing a low threshold will increase sensitivity and decrease false positives. Higher thresholds result in increased specificity, decreased sensitivity, and increased the limit of detection (LOD).

Users can set the threshold according to the situation, such as the presence of an expert, to achieve the optimal results expected from the device.

Meanwhile, 555 clinical specimens from Malawi were used for LOD analysis of the miLab™ as well. In this study, we selected only the positive clinical specimens with low level of parasites, that is, less than 25 infected cells out of 200,000 RBCs. The captured images from the device were reviewed by the experts. We defined a positive result in the miLab™ as at least one malaria parasite-infected RBC above the threshold. The parasitemia level was calculated by converting the number of parasites detected by the miLab™ in 200,000 RBCs to units of 1 µL and estimating 5,000,000 RBCs per µL. The LOD for the point at which a positive result is more than 95% probable by employing probit regression is approximately 31 parasites per µL.

The first generation of malaria diagnosis on the miLab™ was based mainly on the characteristic morphology of *P. falciparum*. The results obtained by a local microscopist, however, confirmed that 4 patients were infected with *P. vivax* and *P. malariae* in addition to *P. falciparum*, based on the expert's microscopy examination. When the expert then reviewed the digital images of the miLab™, various distinct morphologies of *Plasmodium* species were observed. Some already scored over the threshold value even with the current version of the deep-learning algorithm. If the algorithm were to incorporate additional images of various species or stages, the performance of the miLab™ might be further improved and allow classification or detection of *Plasmodium* species. A deep-learning algorithm trained with other types of blood cells would improve the performance of malaria diagnosis by reducing interference caused to WBCs or platelets as well as other types of parasites (e.g., *Trypanosoma cruzi*).

The miLab™ is capable of solving an unmet need in low- and middle-income countries, by providing on-site, sample-to-answer diagnostics for malaria that enables decentralized patient care in the resource-limited setting. For future studies, the miLab™ cartridge can be also applied to the morphological detection of WBCs, because both staining for WBCs and malaria use similar

methods, derived from Romanowsky-type staining (Supplementary Figure 3A)(Choi et al., 2021). Moreover, by modifying the composition of the hydrogels in the cartridge, the miLab™ can prepare different types of sample slides. These include cytology slides with Papanicolaou staining (Supplementary Figure 3B), or tissue sections stained with hematoxylin and eosin (H&E) for histopathology (Supplementary Figure 3C)(Chin et al., 2022). The miLab™ might also be applied to the diagnosis of other infections and detect intestinal parasites (Supplementary Figure 3D) that require microscopic examination without staining ('wet' preparations). The utility of the miLab™ can be extended to diagnose multiple diseases by external training deep-learning algorithms on various types of digital images.

Conclusions

On-site, sample-to-answer malaria diagnosis in the miLab™ enables blood film preparation for embedded deep-learning based malaria detection using digital microscopy images. According to the consistent preparation of the blood film in the miLab™, the accuracy of malaria detection by the miLab™ algorithm was 98.83% for detection of infected RBCs. Clinical validation of the miLab™ demonstrated an overall percent agreement of 92.21% in Malawi. This on-site malaria diagnostic platform can assist experts to review suspected morphology of *Plasmodium* in laboratories and remote locations and suggest remote diagnosis of malaria, especially in resource-limited settings.

Conflict of interest statement

The authors declare the following competing financial interest(s): CYB, YMS, MK, YS, HJL, KHK, YJK, SC, BMW, KHC are currently employees of Noul Co., Ltd. HWL, BK, SH were employees of Noul Co., Ltd. DKL and HB are a member of Scientific Advisory Board (Technical Consultant) in Noul Co., Ltd.

Author Contributions

KHK and CYL conceived conceptualization of the miLab™. CYB, YMS, MK, YS, HJL, HWL, YJK, CK, DKL, SC, BMW, HP contributed development of the experimental methodology. CYB, YMS, MK, YS, KC contributed visualization and investigation of this work. CYL and KC contributed funding acquisition. CYB, YS, MK contributed project administration. CYB, YMS, MK, YS contributed writing the original draft and CYB, YMS, MK, HP, KC contributed writing of the edited manuscript for reviewing.

Acknowledgements

We thank the following associates from Noul Co., Ltd. for contributions to developing hardware, software, and verification of the miLab™: H. Lee, S. Moon, J. Cho, Y. Shin, S. Hong, and R. Choi, D. Ham, O. Bailo, M. J. Seol, Y. Hong, S. Yun, H. Hwang, E. Hwang, S. K. Beak, and J. Choi. We thank J. Lee, H. Park, and J. Shin for monitoring IRB project and Mzuzu Health Centre study team for collecting clinical data. This work was supported by a grant of the Korea Health Technology R&D Project through the Korea Health Industry Development Institute (KHIDI), funded by the Ministry of Health & Welfare, Republic of Korea (grant number: HI18C1685).

References

U.S. President's Malaria Initiative Malawi Malaria Operational Plan FY (2020).

Bae, C. Y., Esmaeili, H., Zamin, S. A., Seol, M. J., Hwang, E., Beak, S. K., et al. (2023). Quantification of solution-free red blood cell staining by sorption kinetics of Romanowsky stains to agarose gels. *Analytical Methods* 15, 5369–5379. doi: 10.1039/D3AY01431B.

Beck, H.-P. (2022). Digital microscopy and artificial intelligence could profoundly contribute to malaria diagnosis in elimination settings. *Front Artif Intell* 5. doi: 10.3389/frai.2022.510483.

Chin, L. K., Li, H., Choi, J.-H., Iwamoto, Y., Oh, J., Min, J., et al. (2022). Hydrogel Stamping for Rapid, Multiplexed, Point-of-Care Immunostaining of Cells and Tissues. *ACS Appl Mater Interfaces* 14, 27613–27622. doi: 10.1021/acsami.2c05071.

Choi, J.-H., Chin, L. K., Woo, B. M., Song, Y., Seol, M. J., Hong, Y., et al. (2021). Hydrogel-Based Stamping Technology for Solution-Free Blood Cell Staining. *ACS Appl Mater Interfaces* 13, 22124–22130. doi: 10.1021/acsami.0c22521.

Das, D., Vongpromek, R., Assawariyathipat, T., Srinamon, K., Kennon, K., Stepniewska, K., et al. (2022). Field evaluation of the diagnostic performance of EasyScan GO: a digital malaria microscopy device based on machine-learning. *Malar J* 21, 122. doi: 10.1186/s12936-022-04146-1.

Fitri, L. E., Widaningrum, T., Endharti, A. T., Prabowo, M. H., Winaris, N., and Nugraha, R. Y. B. (2022). Malaria diagnostic update: From conventional to advanced method. *J Clin Lab Anal* 36. doi: 10.1002/jcla.24314.

Fong Amaris, W. M., Martinez, C., Cortés-Cortés, L. J., and Suárez, D. R. (2022). Image features for quality analysis of thick blood smears employed in malaria diagnosis. *Malar J* 21, 74. doi: 10.1186/s12936-022-04064-2.

Gaston, R. T., and Ramroop, S. (2020). Prevalence of and factors associated with malaria in children under five years of age in Malawi, using malaria indicator survey data. *Heliyon* 6, e03946. doi: 10.1016/j.heliyon.2020.e03946.

Gopakumar, G. P., Swetha, M., Sai Siva, G., and Sai Subrahmanyam, G. R. K. (2018). Convolutional neural network-based malaria diagnosis from focus stack of blood smear images acquired using custom-built slide scanner. *J Biophotonics* 11. doi: 10.1002/jbio.201700003.

He, K., Zhang, X., Ren, S., and Sun, J. (2016). Deep Residual Learning for Image Recognition. in *2016 IEEE Conference on Computer Vision and Pattern Recognition (CVPR)* (IEEE), 770–778. doi: 10.1109/CVPR.2016.90.

Krizhevsky, A., Sutskever, I., and Hinton, G. E. (2012). ImageNet classification with deep convolutional neural networks. in *Advances in Neural Information Processing Systems 25*.

K.T., N., Prasad, K., and Singh, B. M. K. (2022). Analysis of red blood cells from peripheral blood smear images for anemia detection: a methodological review. *Med Biol Eng Comput* 60, 2445–2462. doi: 10.1007/s11517-022-02614-z.

Li, S., Du, Z., Meng, X., and Zhang, Y. (2021). Multi-stage malaria parasite recognition by deep learning. *Gigascience* 10. doi: 10.1093/gigascience/giab040.

Liang, Z., Powell, A., Ersoy, I., Poostchi, M., Silamut, K., Palaniappan, K., et al. (2016). CNN-based image analysis for malaria diagnosis. in *2016 IEEE International Conference on Bioinformatics and Biomedicine (BIBM)* (IEEE), 493–496. doi: 10.1109/BIBM.2016.7822567.

Madhu, G., Mohamed, A. W., Kautish, S., Shah, M. A., and Ali, I. (2023). Intelligent diagnostic model for malaria parasite detection and classification using imperative inception-based capsule neural networks. *Sci Rep* 13, 13377. doi: 10.1038/s41598-023-40317-z.

Meng, X., Ha, Y., and Tian, J. (2022). Neighbor Correlated Graph Convolutional Network for multi-stage malaria parasite recognition. *Multimed Tools Appl* 81, 11393–11414. doi: 10.1007/s11042-022-12098-6.

Mody, R. M., Murray, C. K., Dooley, D. P., Hospenthal, D. R., Horvath, L. L., Moran, K. A., et al. (2006). The Remote Diagnosis of Malaria Using Telemedicine or E-Mailed Images. *Mil Med* 171, 1167–1171. doi: 10.7205/MILMED.171.12.1167.

Molina, A., Alférez, S., Boldú, L., Acevedo, A., Rodellar, J., and Merino, A. (2020). Sequential classification system for recognition of malaria infection using peripheral blood cell images. *J Clin Pathol* 73, 665–670. doi: 10.1136/jclinpath-2019-206419.

Oduola, A. O., Obembe, A., Adelaja, O. J., Adeneye, A. K., Akilah, J., and Awolola, T. S. (2018). Outcome of capacity building intervention for malaria vector surveillance, control and research in Nigerian higher institutions. *Malar J* 17, 193. doi: 10.1186/s12936-018-2344-z.

Oktiyani, N., Muhlisin, A., Roebiakto, E., Norsiah, W., and Mahpolah, M. (2022). Utilization of Alternative Buffer Solutions for Staining Thin Blood smears by the Giemsa, Wright stain and Romanowsky method. *Tropical Health and Medical Research*. doi: 10.35916/thmr.v4i1.76.

Olaf Ronneberger, Philipp Fischer, and Thomas Brox (2015). U-Net: Convolutional Networks for Biomedical Image Segmentation. *Medical Image Computing and Computer-Assisted Intervention (MICCAI)* 9351.

Rajaraman, S., Jaeger, S., and Antani, S. K. (2019). Performance evaluation of deep neural ensembles toward malaria parasite detection in thin-blood smear images. *PeerJ* 7, e6977. doi: 10.7717/peerj.6977.

Shen, D., Wu, G., and Suk, H.-I. (2017). Deep Learning in Medical Image Analysis. *Annu Rev Biomed Eng* 19, 221–248. doi: 10.1146/annurev-bioeng-071516-044442.

Sori, G., Zewdie, O., Tadele, G., and Samuel, A. (2018). External quality assessment of malaria microscopy diagnosis in selected health facilities in Western Oromia, Ethiopia. *Malar J* 17, 233. doi: 10.1186/s12936-018-2386-2.

Tran, T., Minh, L. B., Lee, S.-H., and Kwon, K.-R. (2019). Blood Cell Count Using Deep Learning Semantic Segmentation. *Preprints (Basel)*, 2019090075. doi: 10.20944/preprints201909.0075.v1.

Woo, S., Park, J., Lee, J.-Y., and Kweon, I. S. (2018). CBAM: Convolutional Block Attention Module.

World Health Organization & UNICEF/UNDP/World Bank/WHO Special Programme for Research and Training in Tropical Diseases (2015). *Microscopy for the detection, identification and quantification of malaria parasites on stained thick and thin blood films in research settings (version 1.0): procedure: methods manual*. World Health Organization.

World malaria report 2021 (2021).

Wortsman, M., Ilharco, G., Gadre, S. Y., Roelofs, R., Gontijo-Lopes, R., Morcos, A. S., et al. (2023). Model soups: averaging weights of multiple fine-tuned models improves accuracy without increasing inference time. *ArXiv*, 2203.05482.

Yoon, J., Kwon, J. A., Yoon, S. Y., Jang, W. S., Yang, D. J., Nam, J., et al. (2019). Diagnostic performance of CellaVision DM96 for Plasmodium vivax and Plasmodium falciparum screening in peripheral blood smears. *Acta Trop* 193, 7–11. doi: 10.1016/j.actatropica.2019.02.009.

Zhao, O. S., Kolluri, N., Anand, A., Chu, N., Bhavaraju, R., Ojha, A., et al. (2020). Convolutional neural networks to automate the screening of malaria in low-resource countries. *PeerJ* 8, e9674. doi: 10.7717/peerj.9674.

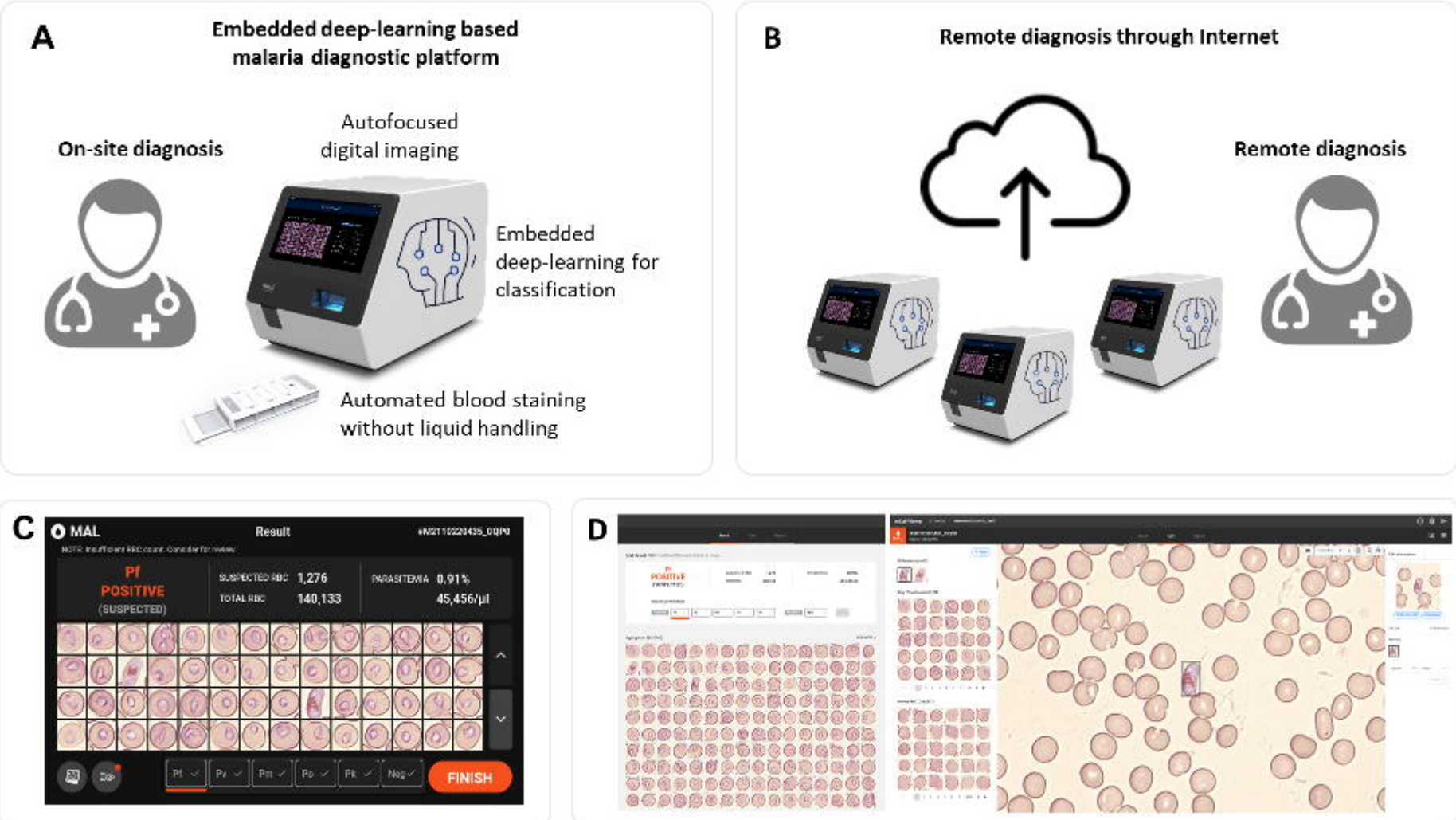
A
Embedded deep-learning based malaria diagnostic platform
On-site diagnosis
Autofocused digital imaging
Embedded deep-learning for classification
Automated blood staining without liquid handling
B
Remote diagnosis through Internet
Remote diagnosis
C
MAL
Result
Pf
POSITIVE
(SUSPECTED)
SUSPECTED RBC 1,276
TOTAL RBC 140,133
PARASITEMIA 0.91%
45,456/µl
FINISH
D

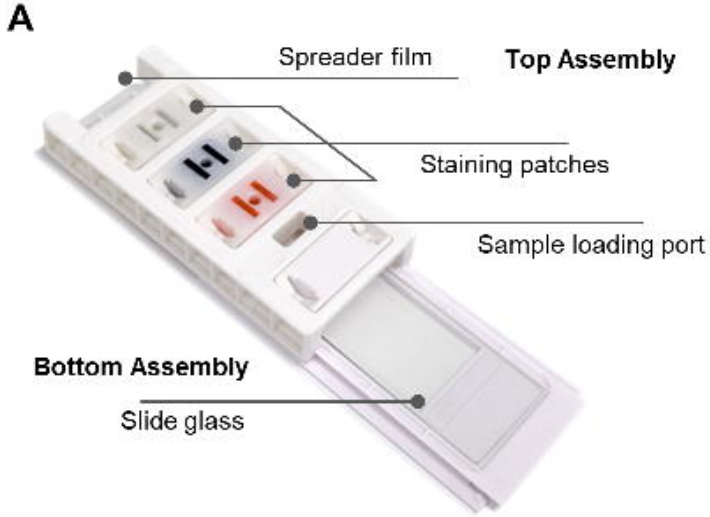

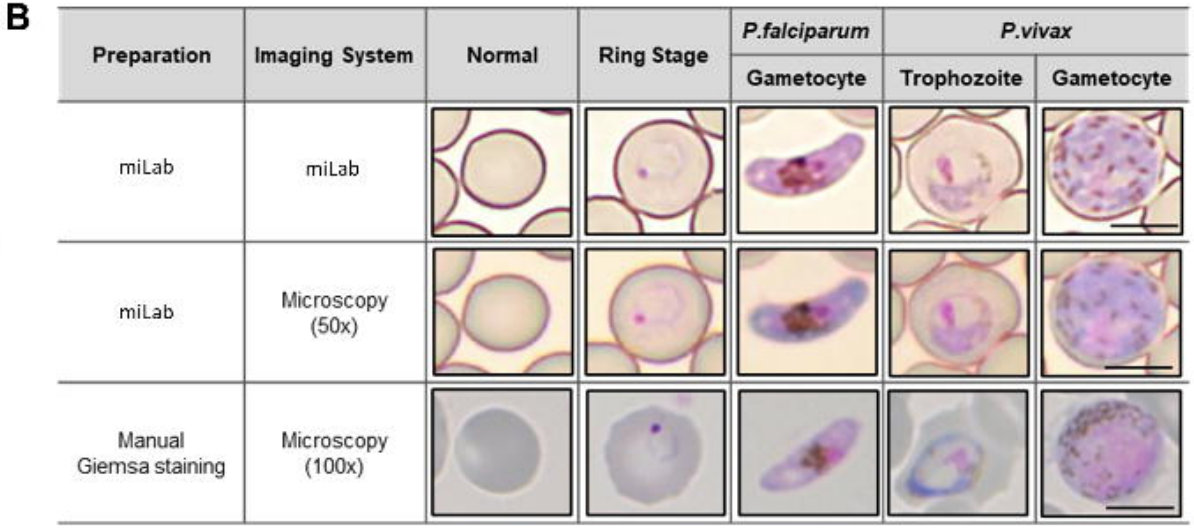

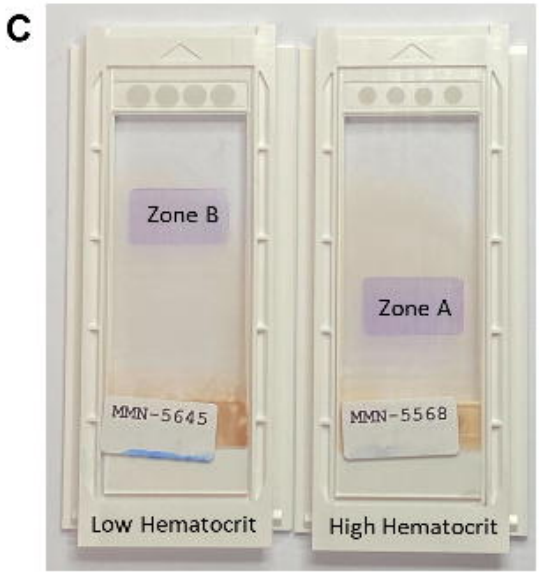

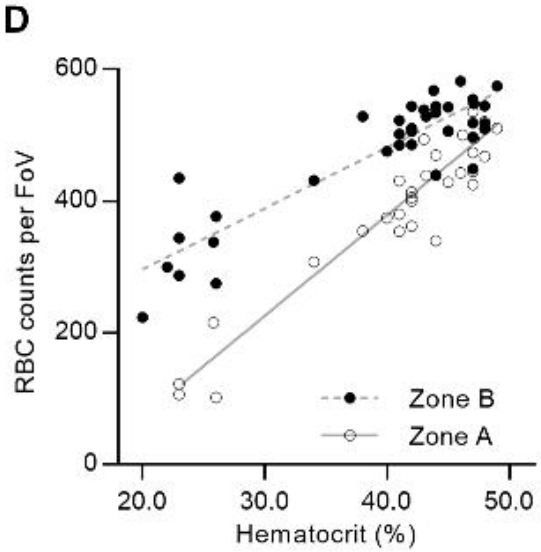

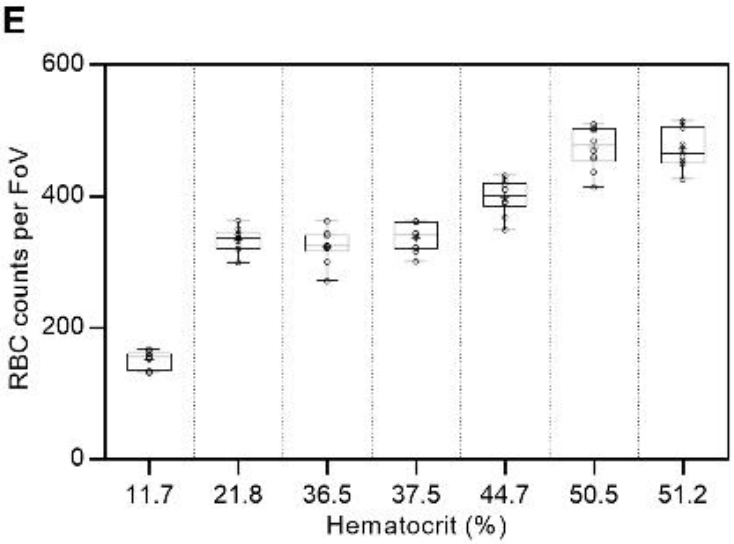

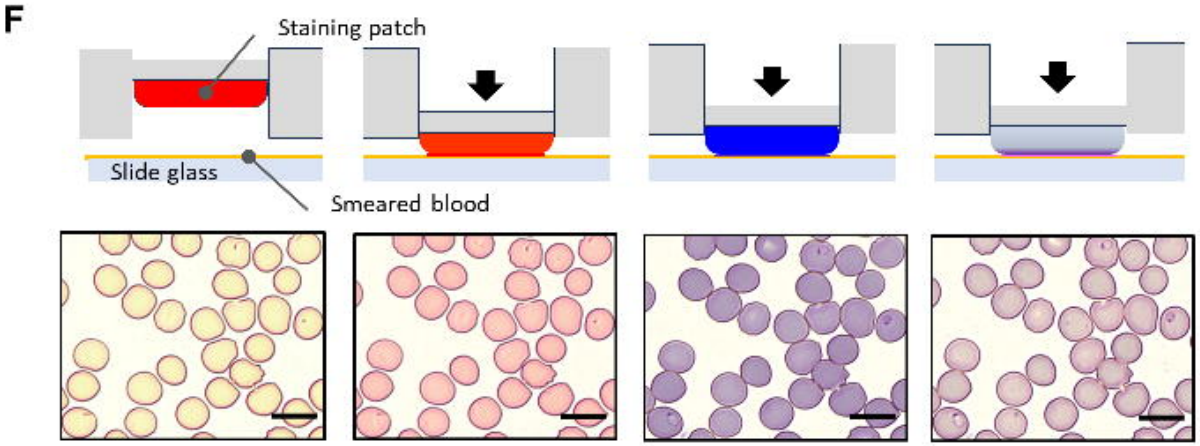

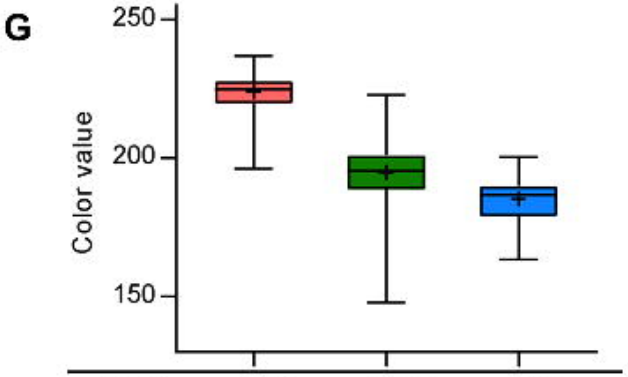

Color	Red	Green	Blue
%CV	2.55	4.71	3.42

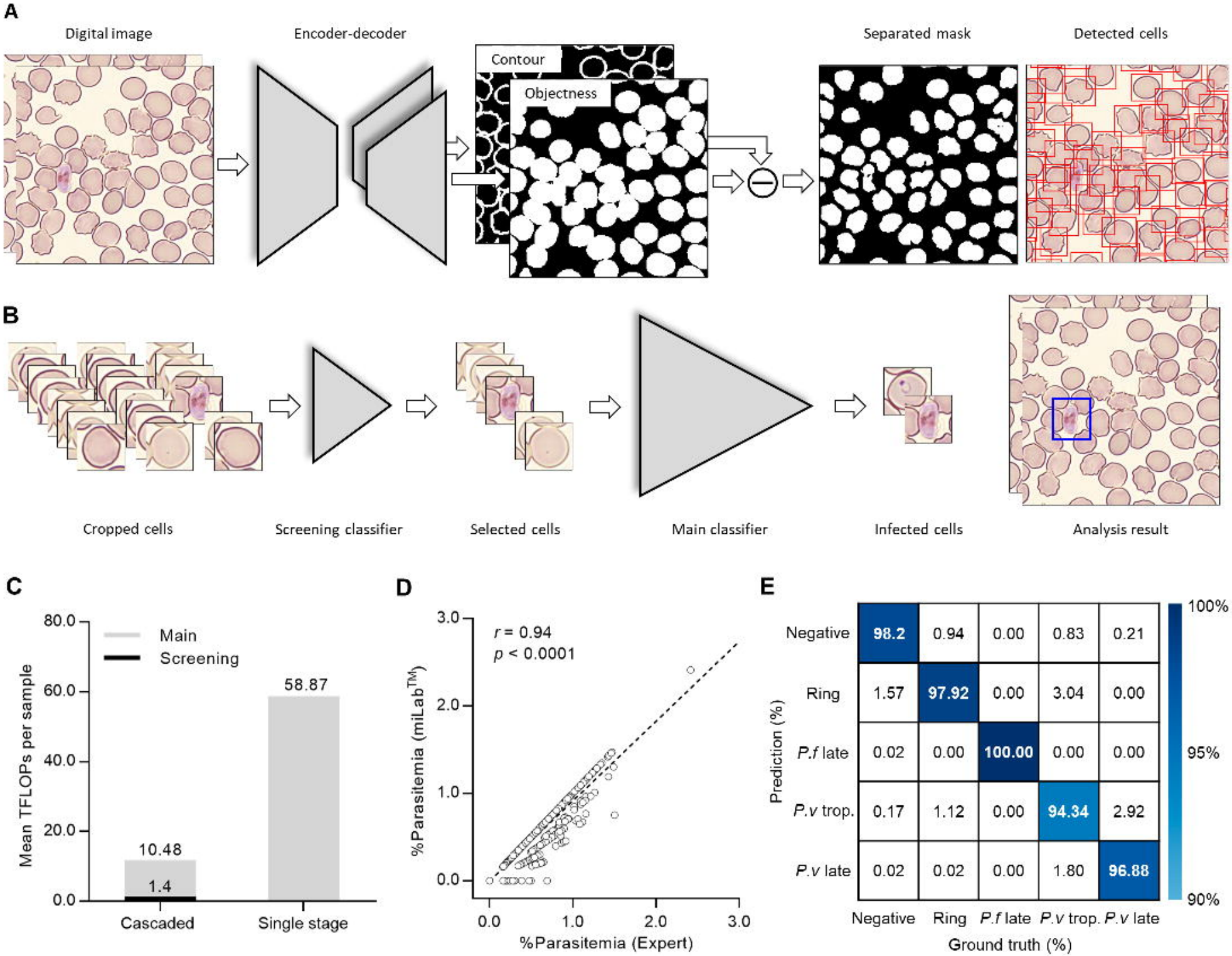
A
Digital image
Encoder-decoder
Contour
Objectness
Separated mask
Detected cells
B
Cropped cells
Screening classifier
Selected cells
Main classifier
Infected cells
Analysis result
C
Main
Screening
Mean TFLOPs per sample
80.0
60.0
40.0
20.0
0.0
10.48
1.4
58.87
Cascaded
Single stage
D
r = 0.94
p < 0.0001
%Parasitemia (miLab™)
%Parasitemia (Expert)
0.0
1.0
2.0
3.0
E
Prediction (%)
Ground truth (%)
Negative
Ring
P.f late
P.v trop.
P.v late
98.2 0.94 0.00 0.83 0.21
1.57 97.92 0.00 3.04 0.00
0.02 0.00 100.00 0.00 0.00
0.17 1.12 0.00 94.34 2.92
0.02 0.02 0.00 1.80 96.88
100%
95%
90%

A

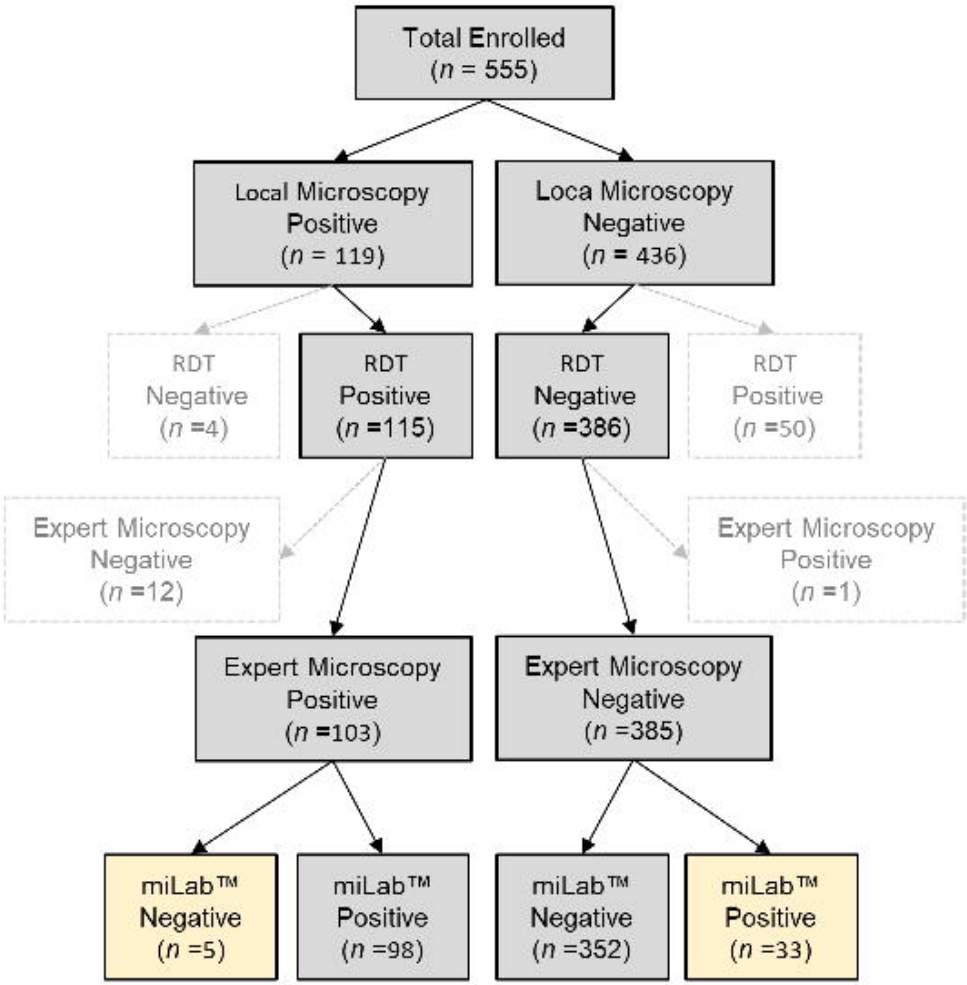

B

Reference method: both Microscopy and RDT (*n* = 488)

miLab™	Positive	Negative
Positive	98	33
Negative	5	352
OPA% (95% CI)	92.21 (89.47–94.43)	
PPA% (95% CI)	95.15 (89.03–98.41)	
NPA% (95% CI)	91.43 (88.17–94.03)	
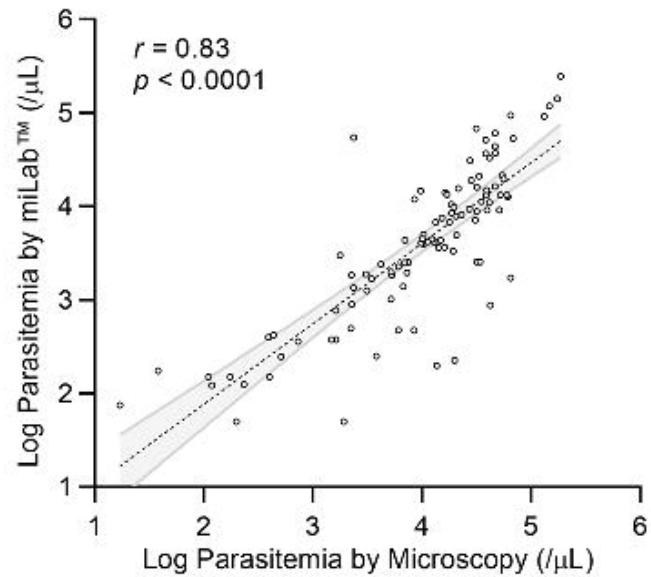
C